REPORT No. 465

DETERMINATION OF THE THEORETICAL PRESSURE DISTRIBUTION FOR TWENTY AIRFOILS

By I. E. Garrick

SUMMARY

This report gives the theoretical distribution of pressure at lift coefficients of 0, 0.5, 1.0, and 1.5 for 20 airfoils, calculated on the basis of a rigorous potential theory of arbitrary airfoils. It also provides tables from which the characteristics of the airfoils for any angle of attack in 2-dimensional potential flow are readily calculable. The theoretical values of the angles of zero lift, the lift and moment coefficients, and the ideal angles of attack are listed and some comparisons with experiment are indicated. Some of the well-known characteristics and properties of airfoils are accounted for in terms of the theoretical pressure-distribution curves. Qualitative deductions are made concerning the causes of breakdown of potential flow and the efficiency of the airfoil in viscous flow. The results presented may be of value in predicting structural loads and also in a correlation of theoretical pressure gradients with profile resistance.

INTRODUCTION

Until recently the theoretical distribution of pressure around airfoils could be determined only for the so-called "theoretical" airfoils. Indeed, only in the particular case of the Joukowsky airfoils is the calculation not unduly laborious. (See references 1 and 2.) The theoretical airfoils, which are defined by special mathematical transformations, have, however, seldom been employed in practice. Their use in a precise study of pressure distribution has in fact been due more to necessity than to desire. The distribution of pressure for mathematically "thin" airfoils (i.e., the airfoil is represented by the mean-camber line) can be obtained, at least approximately, by the processes given by Munk, Glauert, and Theodorsen (references, 3, 4, and 5). In another report (reference 6) Theodorsen developed a theory readily applicable to arbitrary airfoils. This theory was extended by Theodorsen and Garrick in reference 7, in a report which gives a unified treatment of the 2-dimensional potential flow around airfoils of *any* shape. The treatments given in references 6 and 7 avoid approximations in the analysis, and are referred to for details of the underlying theory of the results of the present paper.

The differences exhibited by airfoils in potential flow, as well as the differences between the actual and ideal cases for a particular airfoil, can, of course, be critically studied only if the ideal case is known. Furthermore, it is only on this basis that the assumptions of the theory itself can be critically analyzed and modified. It is therefore believed that an existing gap in aerodynamical literature will be, to some extent, bridged by the publishing in the present paper of convenient tables and curves of the theoretical results for a number of commonly used and related airfoils.

A knowledge of the theoretical distribution of pressure for an airfoil is, undoubtedly, a major factor in making it ultimately possible to predict accurately the behavior and efficiency of the airfoil under actual conditions, for the theoretical changes along the surface from pressure to velocity and from velocity to pressure are very significant in the determination of the drag characteristics. Knowledge of the theoretical results is of considerable value, too, for guiding experimental work whenever the measurements are rather critical, and such information also directs attention to the significance and interpretation of differences between theory and experiment.

Unfortunately, because of lack of sufficient accurate experimental data, comparison cannot be made directly with wind-tunnel results except in a few cases. In reference 7 an interesting comparison was given between theory and experiment of the pressure distribution around the N.A.C.A.-M6 airfoil at 12 different angles of attack. Reference 8 may be referred to for qualitative experimental results for five additional airfoils. A more accurate experimental study of pressure distributions is in progress at the present time at the N.A.C.A. laboratories.

A part of the following work was undertaken at the request of the Bureau of Aeronautics, Navy Department, for use in work on structural loads.

In making the calculations the author was ably assisted by Miss Alyce V. Rudeen, of the Committee's staff.

SUMMARY OF FORMULAS USED

The formulas used to obtain the results presented in the tables and curves are developed in references 6 and 7. A sample calculation for the N.A.C.A.-M6 airfoil with a comparison with experimental results, as well as explanatory figures and diagrams illustrating the use of the formulas, is given in reference 7. The following list presents the symbols employed and their definitions:

	SYMBOL	DEFINITION
(1)	(x, y)	See discussion of the choice of axes in a following paragraph.
(2)	θ	$2\sin^2\theta = p+\sqrt{p^2+y^2}$ where $p=1-\left(\frac{x}{2}\right)^2-\left(\frac{y}{2}\right)^2$
(3)	ψ	$2\sinh^2\psi = -p+\sqrt{p^2+y^2}$. Since y is generally small for airfoils, the following equation may be preferable: $\sinh\psi=\frac{y}{2\sin\theta}$. Near the leading (or trailing) edge ψ is given approximately by $\psi=\sqrt{\frac{\sigma}{2}}$ where σ is the radius of curvature at the leading (or trailing [1]) edge.
(4)	ϵ	$\epsilon(\phi')=-\frac{1}{2\pi}\int_0^{2\pi}\psi(\phi)\cot\frac{\phi-\phi'}{2}\,d\phi$ See appendix[2] of reference 7 for method of evaluation.
(5)	ϵ'	Obtained graphically from the ϵ, θ curve. (Denoted $\frac{d\epsilon}{d\theta}$ in reference 7.)
(6)	ψ'	Obtained graphically from the ψ, θ curve. (Denoted $\frac{d\psi}{d\theta}$ in reference 7.)
(7)	ϕ	$\phi=\theta+\epsilon$.
(8)	ψ_0	A constant: $\psi_0=\frac{1}{2\pi}\int_0^{2\pi}\psi(\phi)\,d\phi$
(9)	α	Angle of attack with respect to the x axis.
(10)	β	The angle of zero lift, given by the value of ϵ for $\theta=\pi$.
(11)	k	$k=\frac{e^{\psi_0}(1+\epsilon')}{\sqrt{(\sinh^2\psi+\sin^2\theta)(1+\psi'^2)}}$ Note: k is independent of the angle of attack.
(12)	$\frac{v}{V}$	The ratio of the local velocity at the airfoil surface to the uniform stream velocity: $\frac{v}{V}=k[\sin(\alpha+\phi)+\sin(\alpha+\beta)]$.
(13)	$\frac{p}{q}$	The ratio of the local superstream pressure to the dynamic pressure (the term "superstream pressure" is used to designate the difference of the local pressure and the static pressure in the undisturbed uniform stream): $\frac{p}{q}=1-\left(\frac{v}{V}\right)^2$ and $q=\frac{1}{2}\rho V^2$.
(14)	c	The segment of the x axis intercepted by the airfoil boundary.
(15)	C_L	The lift coefficient $C_L=\frac{L}{\frac{1}{2}\rho c V^2}=\frac{8\pi e^{\psi_0}}{c}\sin(\alpha+\beta)$
(16)	F	A point designated the "focus" of the airfoil. We may first define the complex constants c_1 and c_2 as $c_1=me^{i\delta}=A_1+iB_1$ $=\frac{e^{\psi_0}}{\pi}\int_0^{2\pi}\psi(\phi)\,(\cos\phi+i\sin\phi)\,d\phi$ $c_2=A_2+iB_2$ $=\frac{e^{2\psi_0}}{\pi}\int_0^{2\pi}\psi(\phi)(\cos 2\phi+i\sin 2\phi)\,d\phi$ Then writing $b^2e^{2i\gamma}=1+\frac{c_1^2}{2}+c_2$ we have $b^4=\left(1+\frac{A_1^2-B_1^2}{2}+A_2\right)^2+(A_1B_1+B_2)^2$ and $\gamma=\frac{1}{2}\tan^{-1}\frac{A_1B_1+B_2}{1+\frac{A_1^2-B_1^2}{2}+A_2}$ Then the complex coordinate of F is $z_F=(x+iy)_F=me^{i\delta}+\frac{b^2}{e^{\psi_0}}e^{i(2\gamma-\beta)}$
(17)	M_F	The moment at F is constant for all angles of attack: $M_F=2\pi\rho b^2V^2\sin 2(\gamma-\beta)$
(18)	C_{MF}	The moment coefficient referred to the point F: $C_{MF}=\frac{M_F}{c^2q}=4\pi\frac{b^2}{c^2}\sin 2(\gamma-\beta)$
(19)	α_I	The "ideal" angle of attack: $\alpha_I=-\frac{\epsilon_N+\epsilon_T}{2}$ where ϵ_N and ϵ_T denote, respectively, the values of ϵ at the nose and tail; i.e., for $\theta=0$ and $\theta=\pi$, respectively.

The ideal angle of attack for thin airfoils has been defined by Theodorsen (reference 5) as that angle for which the front stagnation point is at the leading edge.

[1] For airfoils whose trailing edges are not uniquely defined, it is convenient to consider the trailing edge as formed by an arc of very small radius of curvature, and to fair in the ψ,θ curve near $\theta=\pi$.

[2] A convenient 20-point method is given here which in practice is quite sufficient. However, any number may be used, or any interval which appears to be critical may be subdivided and treated separately.

At this angle of attack large velocity gradients at the leading edge are avoided and the profile drag is at, or very near, its minimum value. The definition can be naturally extended to actual airfoils to designate that angle of attack for which the front stagnation point is at the foremost edge of the mean-camber line. However, as pointed out by Theodorsen, the effective mean-camber line of a thick airfoil actually alters with change of angle of attack, and the ideal angle of attack for a thick airfoil represents an average of a range of angles for which the profile drag is very near its minimum.

PROCEDURE AND ACCURACY OF THE CALCULATIONS

In order to avoid possible confusion it may be well to state beforehand that the term "chord" is used in this paper as synonymous with the segment of the x axis intercepted by the airfoil. The "standard chord" in terms of which the airfoil is usually empirically defined does not, in general, coincide with this above-defined chord. The angle between the x axis as chosen and the standard chord is designated λ and is listed in table I. (See also fig. 1.)

In the procedure of the calculations, the axes of coordinates are first chosen in a definite convenient way, since the ease and rapidity of convergence of further evaluations depend considerably on the choice of axes (references 6 and 7). This choice may be made as follows: If the distance between the leading edge of the airfoil and the center of curvature of the leading edge is bisected at E (the coordinates of E are (2, 0)), and the same is done for the trailing edge at E' (the coordinates of E' are $(-2, 0)$), then the x axis should pass through EE' and the origin bisects the distance EE'. However, *small* variations from this particular choice of axis and origin do not noticeably influence the ease of calculation.[3] The quantities given in the headings of table II are directly calculated in terms of x and y by means of the formulas previously listed. The angle of attack corresponding to a given value of the lift coefficient may be obtained from (15), in which c is $X_N - X_T$, where X_N and X_T denote the abscissas of the leading edge and trailing edge, respectively. The moment coefficient C_{M_F} may be obtained from (18), in which the constants b^2 and γ are obtained from (16) by graphical integration of the $\psi \sin \phi$, $\psi \cos \phi$, $\psi \sin 2\phi$, and $\psi \cos 2\phi$ curves.

The ordinates of the airfoil are given empirically to hundredths of a percent of the standard chord for 16 stations of the upper and lower surfaces respectively. The quantities x, y, ψ, and θ are defined to the same degree of accuracy. The ψ, θ curve is thus a faired curve through 32 points and ϵ (θ) is estimated to be of the same order of accuracy as $\psi(\theta)$. The derivatives ϵ' and ψ', being determined graphically, admit of a possible small error which, however, causes an error in k of probably less than 2 percent. The angle of zero lift, or the value of ϵ for $\theta = \pi$, may perhaps be in error as much as 15′, but the influence of this possible error on the theoretical pressure-distribution curves for fixed values of C_L is negligible.

The numerical data for the Clark Y airfoil are presented in table II. The distribution of velocity and pressure for any angle of attack or at any lift coefficient, as well as other theoretical characteristics, are obtained with a minimum of effort from this table. Similar tables for the remaining airfoils are omitted here for reasons of economy in printing and also because it is not known how general the interest in them will be. They are available on request from the National Advisory Committee for Aeronautics.

DISCUSSION

Although the airfoils chosen in this paper are mainly conventional airfoils (fig. 1) and not extremely radical types, it is nevertheless possible to isolate some of the individual effects of change of shape and compare these with experimental results. It is believed, however, that future experimental work on radical and less conventional shapes, for which the theoretical results are readily available (see, for example, reference 7, p. 31), will enable the isolation and analysis of effects which are probably masked and unemphasized in conventional types.

We may first make some general comments regarding the curves of theoretical pressure distribution given in the following pages. In each figure the abscissa represents the location of a point of the airfoil surface in percent chord and the ordinate gives the quantity p/q, the ratio of the local superstream pressure to the dynamic pressure q. It may be noted that negative values of p/q are plotted upwards. This is an arbitrary convention and is made because it is more readily associated with the upper surface of the airfoil, which for ordinary angles of attack is the surface of suction or negative pressure. In figures 2 to 21, inclusive, it may be noted that the points of the curves above the zero, or normal pressure, line represent suction; that is, velocities, greater than V. Positive values of p/q denote pressures greater than normal static pressure; i.e., $v < V$. The stagnation points at which $v = 0$ correspond to $\frac{p}{q} = 1$.

Effect of compressibility.—In figure 22 there is shown for convenience a curve of the dynamic pressure q in inches of water and in pounds of force per square foot against velocity in miles per hour. The values given correspond to atmospheric conditions at 2,000 feet altitude and 0° C. For the ordinary velocity range of aircraft, say from 45 to 200 miles per hour, q varies from about 1 to 20 inches of water. For very great velocities the effect of compressibility of the air

[3] Notice, however, that we have chosen the rear stagnation point on the x axis at $\theta = \pi$, thus fixing the calculation by the Kutta condition. Strictly speaking, then, the x axis should be chosen in the unique manner indicated above (this has been done for the airfoils treated here), for, if another axis is chosen, the rear stagnation point must be properly relocated with respect to it, causing a change in the angle of zero lift with respect to the new axis.

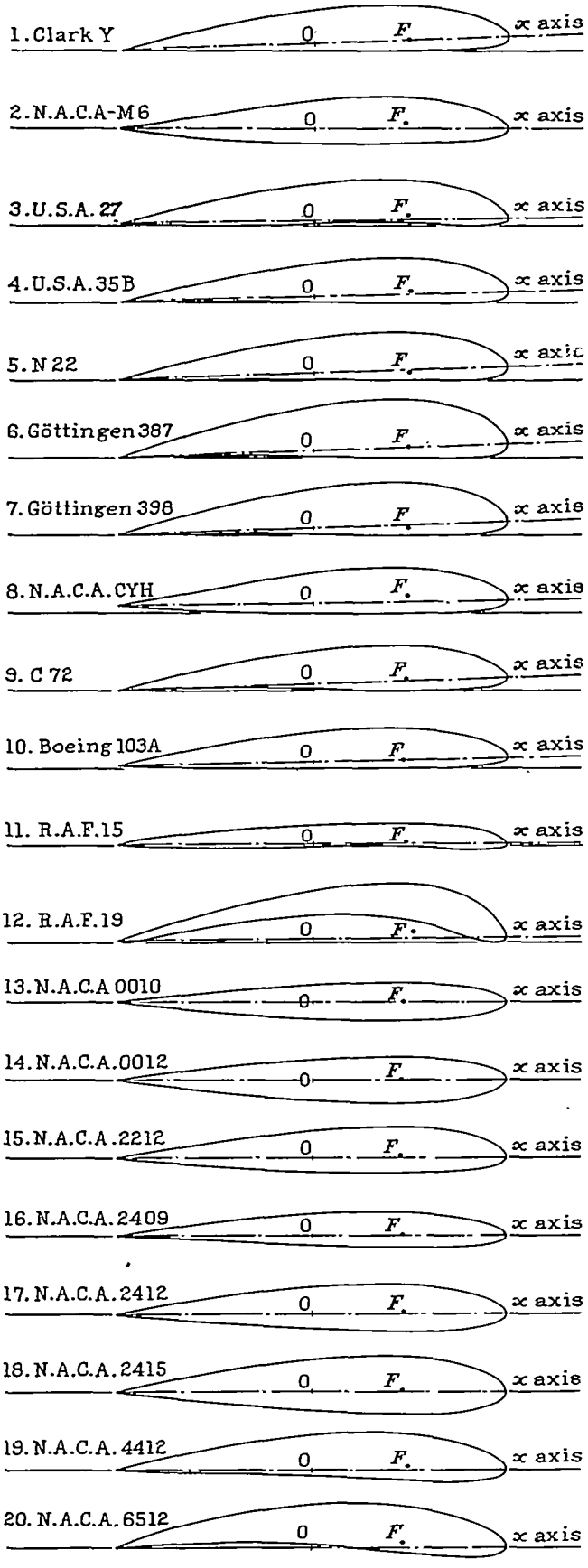

FIGURE 1.—The 20 airfoils chosen, showing axes and location of F.

becomes significant and the potential-theory characteristics based on an assumption of incompressibility may be considerably altered. However, as is pointed out by Glauert (reference 10), the compressibility of air has minor influence for velocities under 0.5 the velocity of sound, or ordinarily about 350 miles per hour. However, it should be noted that at certain angles of attack the local velocity may be as much as two or more times the stream velocity. Thus, for very great velocities, the strong suction in the region of the peak pressures may introduce radical changes in the flow, as the compressibility properties of the fluid become important. This effect is associated with Mach's Number (v/c, where c is the velocity of sound in the medium), and the ordinary Reynolds Number alone is not a safe criterion for scale effect. The potential theory yet remains to be properly modified for the effect of compressibility. Reference 9 gives some experimental results of the distribution of pressure over airfoils for very high speeds. The maximum negative pressure (or suction) obtained in this reference was 37 cm of mercury.

Pressure gradients.—From the concept of the ideal angle of attack we are led to expect that the thinner the airfoil at the leading edge the greater the velocities near the leading edge for angles different from α_I. This expectation is confirmed by the large negative values of p/q attained by the R.A.F. 15 and the N.A.C.A. 0010, 0012, and 2409 airfoils. In particular, the pressure on the N.A.C.A. 0010 reaches $-11q$ for lift coefficient $C_L=1.5$, whereas the somewhat thicker N.A.C.A. 0012 reaches $-7q$ at the same lift coefficient. In practice, the value of C_{Lmax} for the N.A.C.A. 0012 is somewhat greater than that for the N.A.C.A. 0010. Results of force tests of the airfoils treated in this paper are presented in references 11, 12, and 13.

The large gradient of pressure behind the negative peak pressure is very significant for the breakdown of potential flow. The deceleration of fluid becomes so rapid that fluid is piled up at the trailing edge and the flow no longer separates precisely at the trailing edge but breaks off along the upper surface. The flow along the lower surface undergoes but little change at high angles of attack except that, after the breakdown of potential flow has occurred, the pressure at the trailing edge may be somewhat negative instead of positive.

The change from the front stagnation point to maximum velocity occurs within a very small space interval, and all indications are that frictional losses are practically negligible while the fluid is accelerating, as compared with losses when deceleration occurs. The fluid follows the surface boundary more easily in the change from pressure energy to kinetic energy than vice versa. This fact is also abundantly confirmed by experiments with nozzles and venturi tubes. For

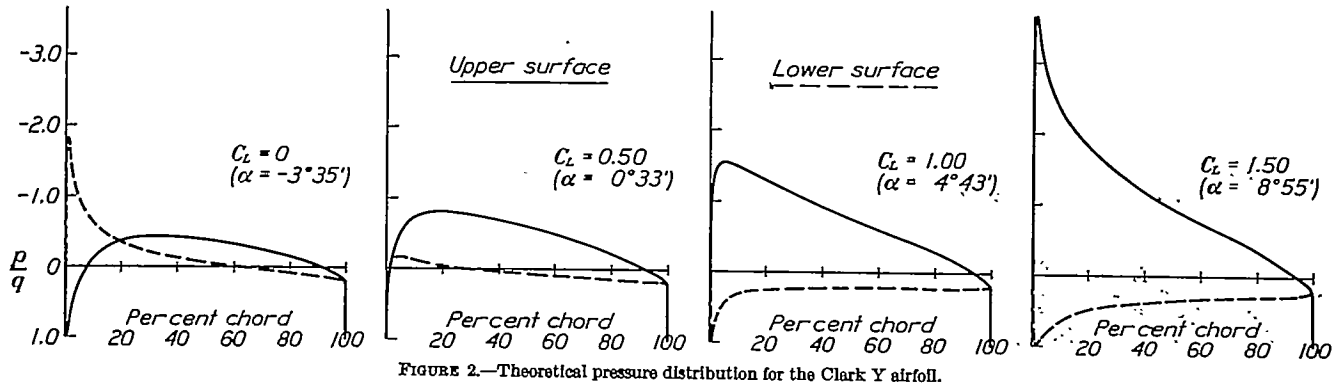

FIGURE 2.—Theoretical pressure distribution for the Clark Y airfoil.

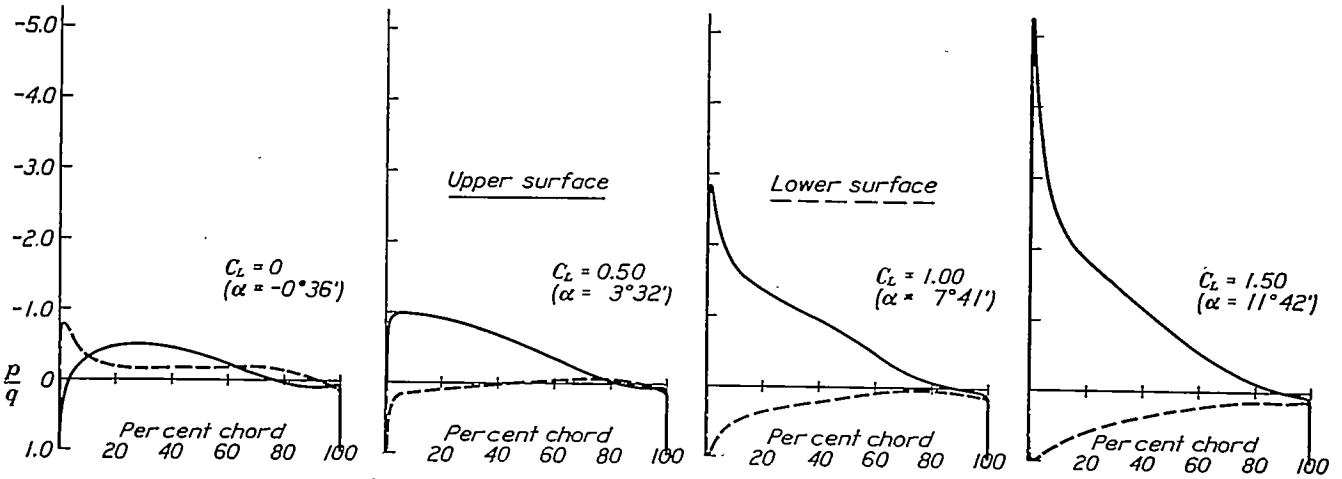

FIGURE 3.—Theoretical pressure distribution for the N.A.C.A.-M6 airfoil.

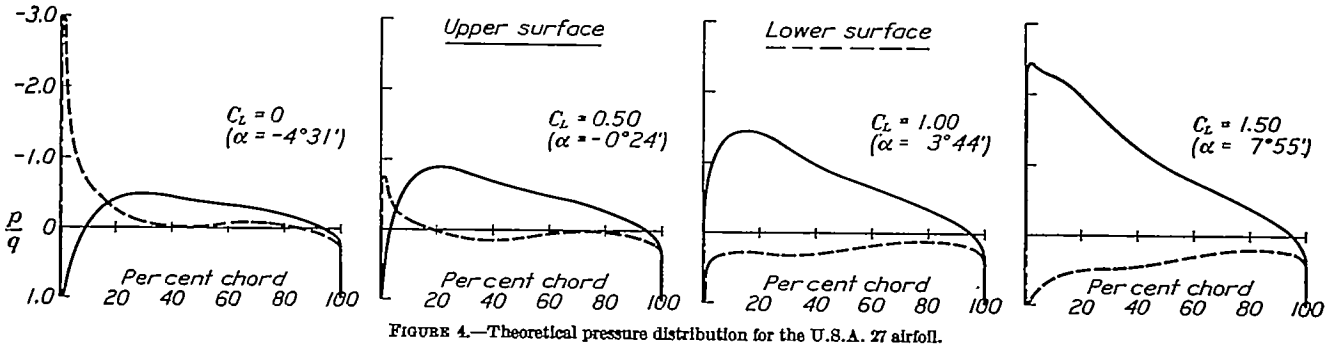

FIGURE 4.—Theoretical pressure distribution for the U.S.A. 27 airfoil.

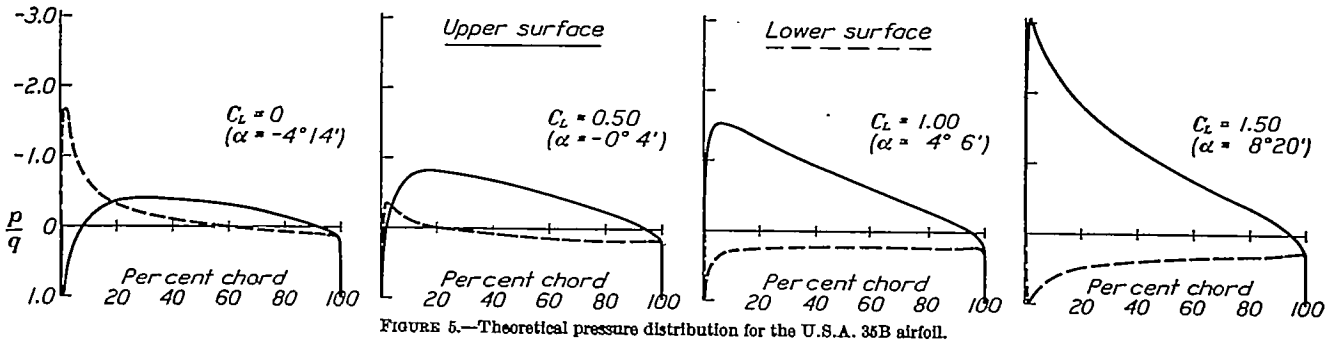

FIGURE 5.—Theoretical pressure distribution for the U.S.A. 35B airfoil.

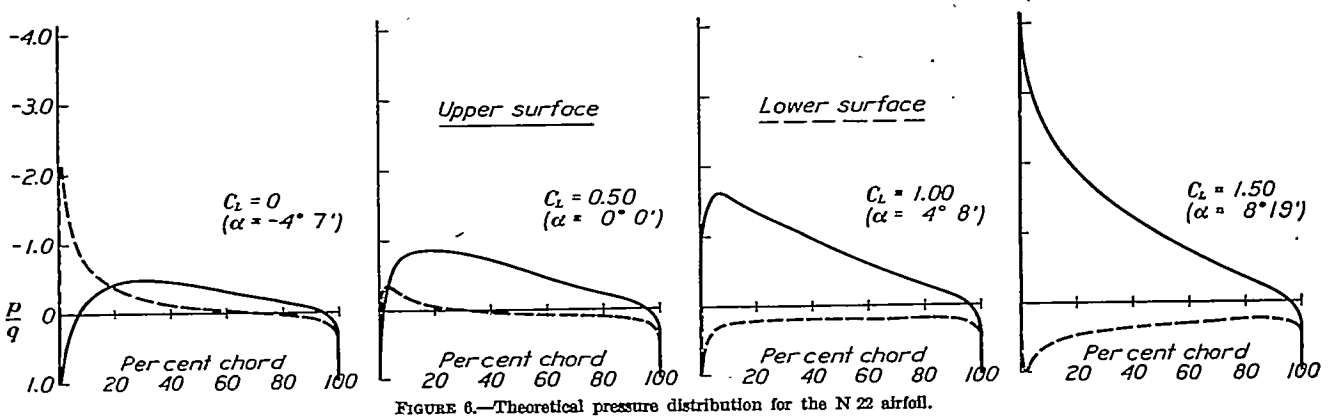

FIGURE 6.—Theoretical pressure distribution for the N 22 airfoil.

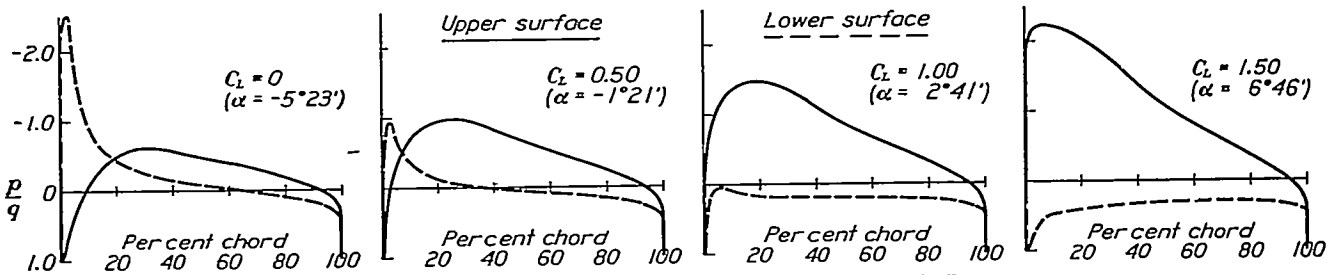

FIGURE 7.—Theoretical pressure distribution for the Göttingen 387 airfoil.

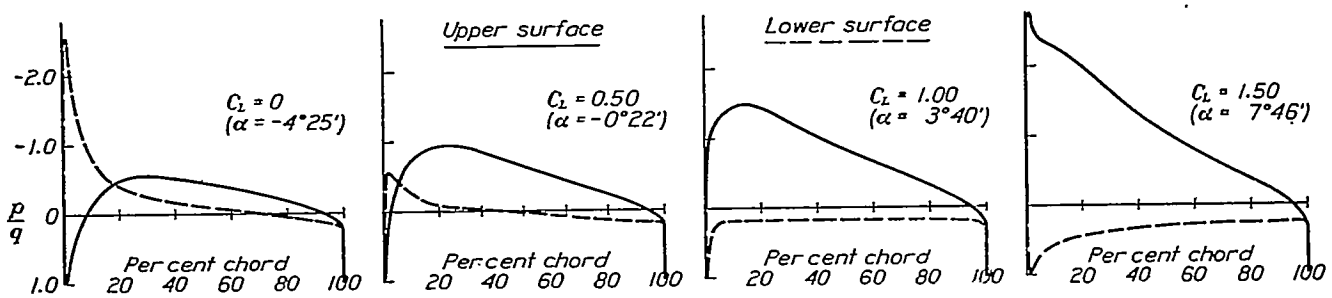

FIGURE 8.—Theoretical pressure distribution for the Göttingen 398 airfoil.

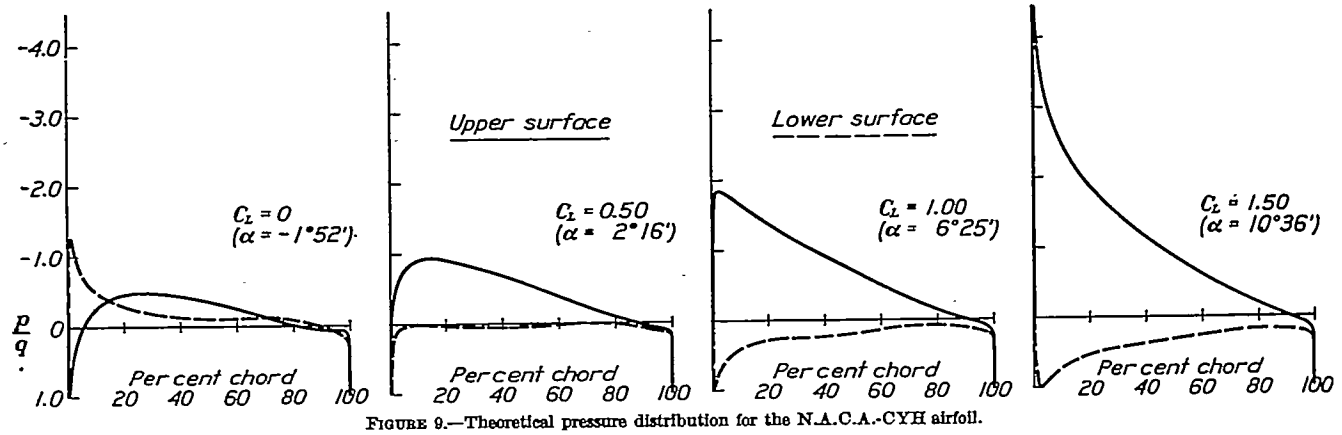

FIGURE 9.—Theoretical pressure distribution for the N.A.C.A.-CYH airfoil.

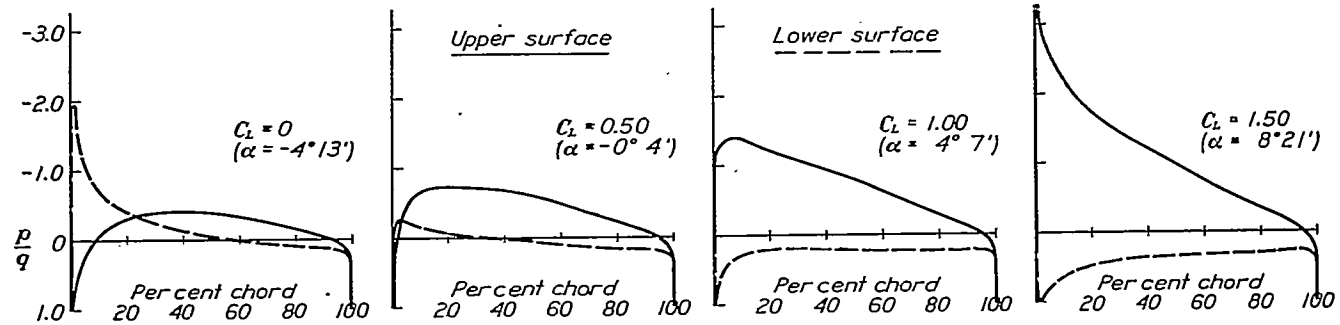

FIGURE 10.—Theoretical pressure distribution for the C 72 airfoil.

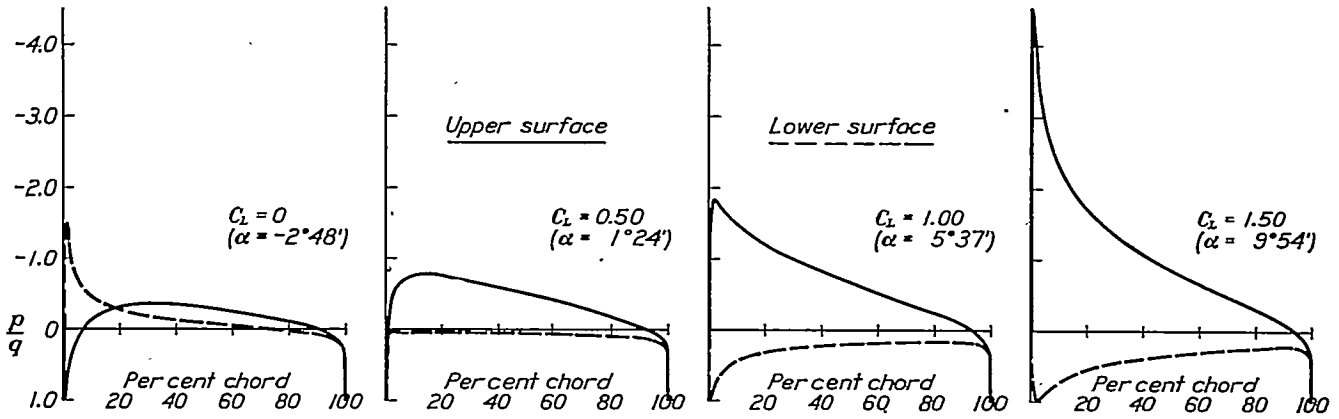

FIGURE 11.—Theoretical pressure distribution for the Boeing 103-A airfoil.

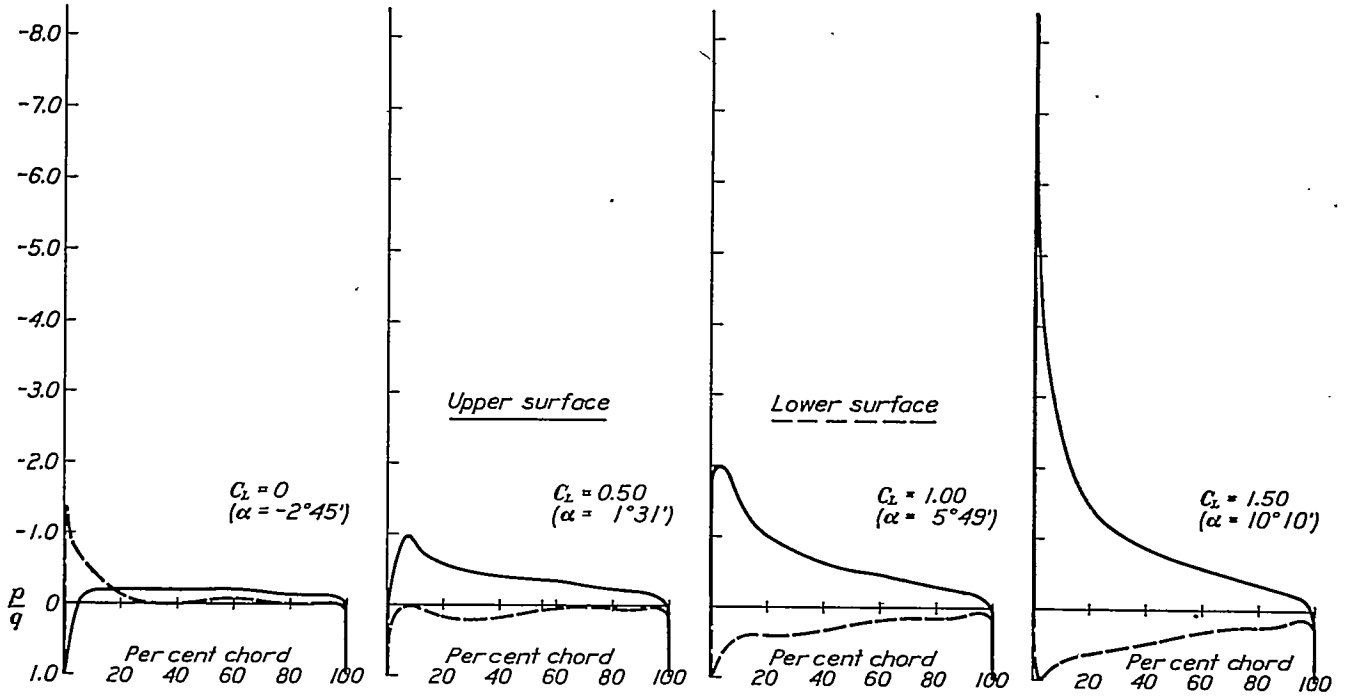

FIGURE 12.—Theoretical pressure distribution for the R.A.F. 15 airfoil.

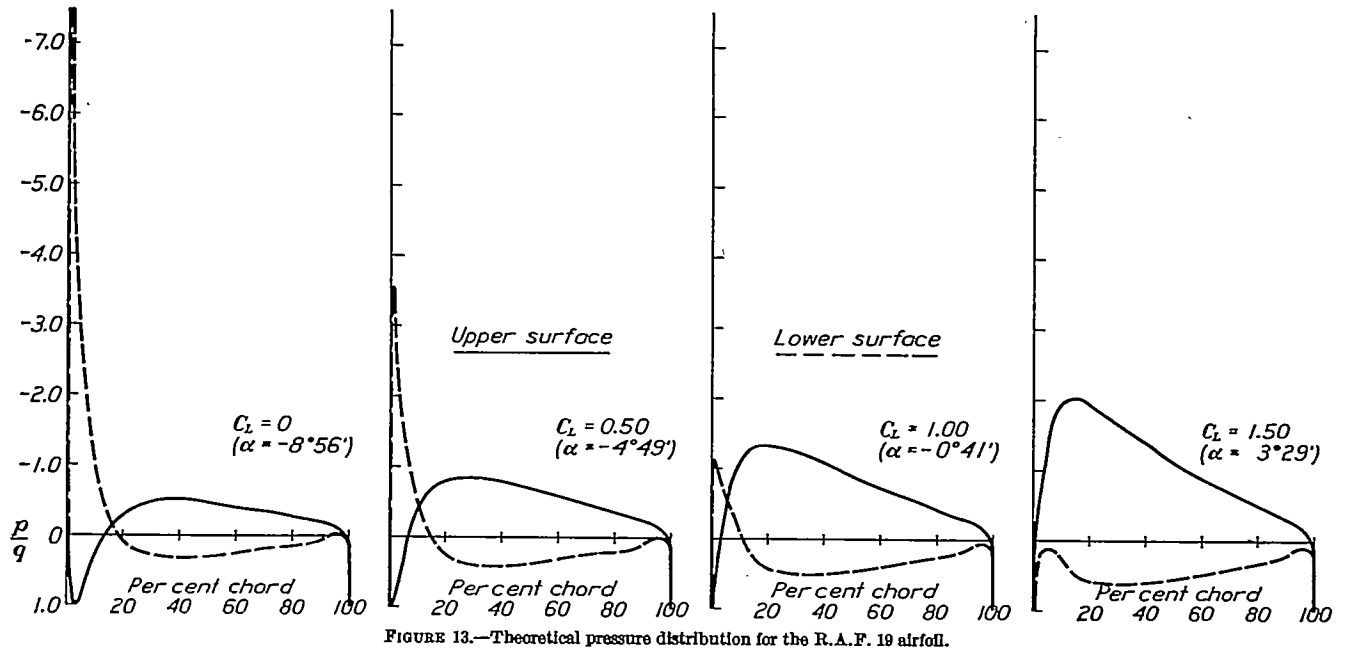

FIGURE 13.—Theoretical pressure distribution for the R.A.F. 19 airfoil.

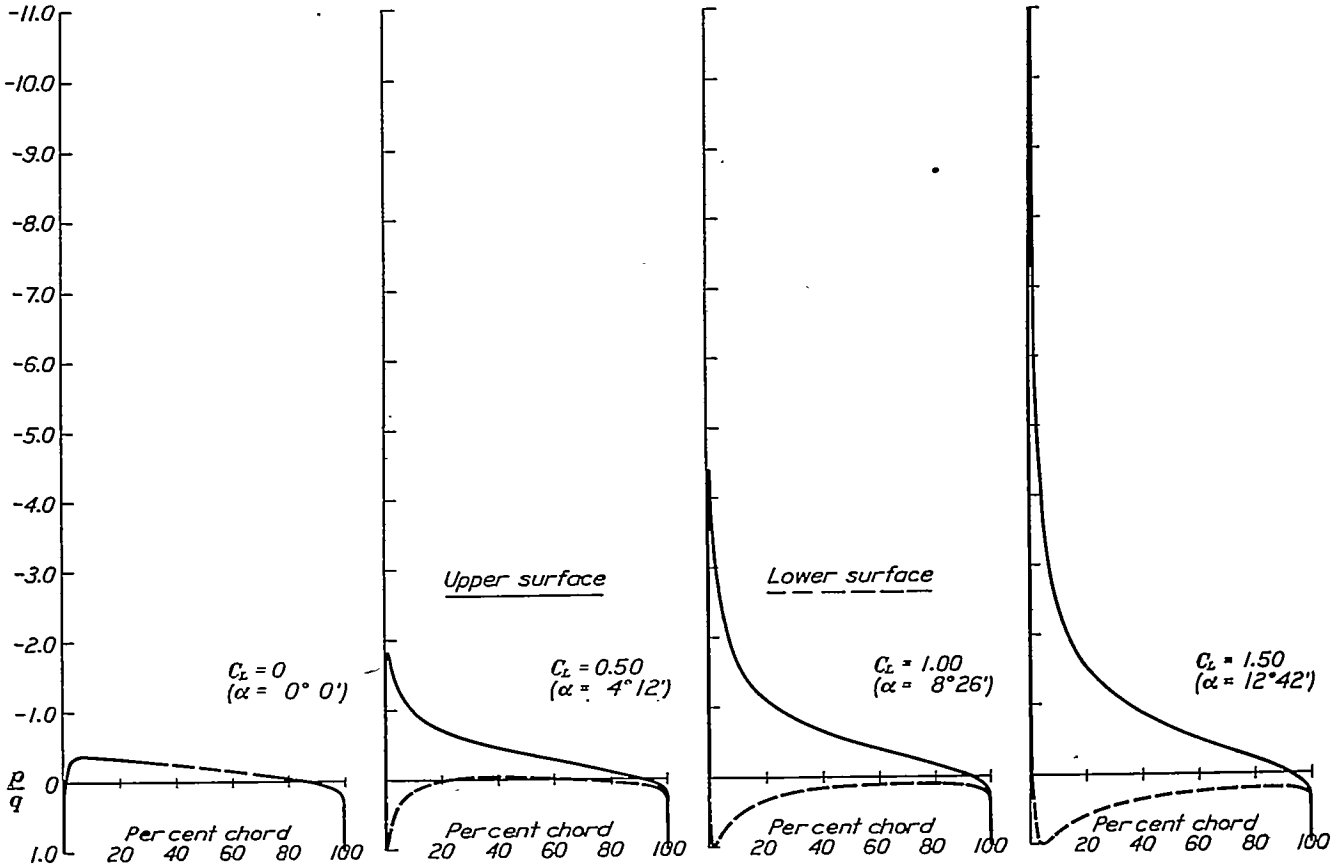

FIGURE 14.—Theoretical pressure distribution for the N.A.C.A. 0010 airfoil.

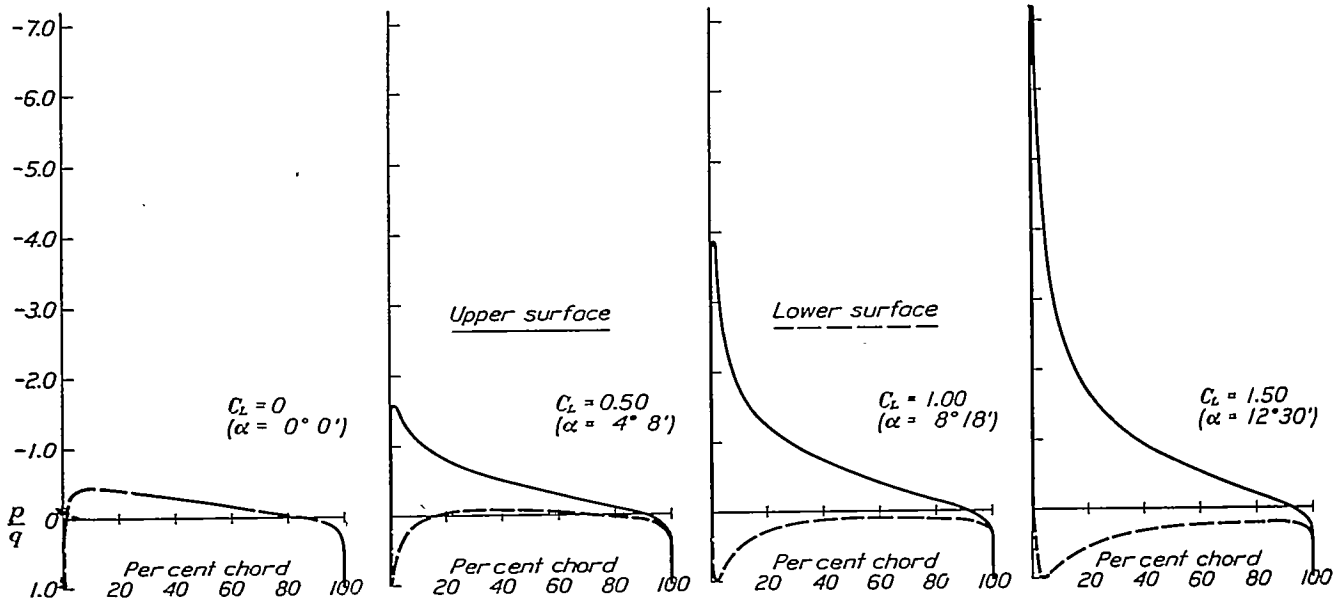

FIGURE 15.—Theoretical pressure distribution for the N.A.C.A. 0012 airfoil.

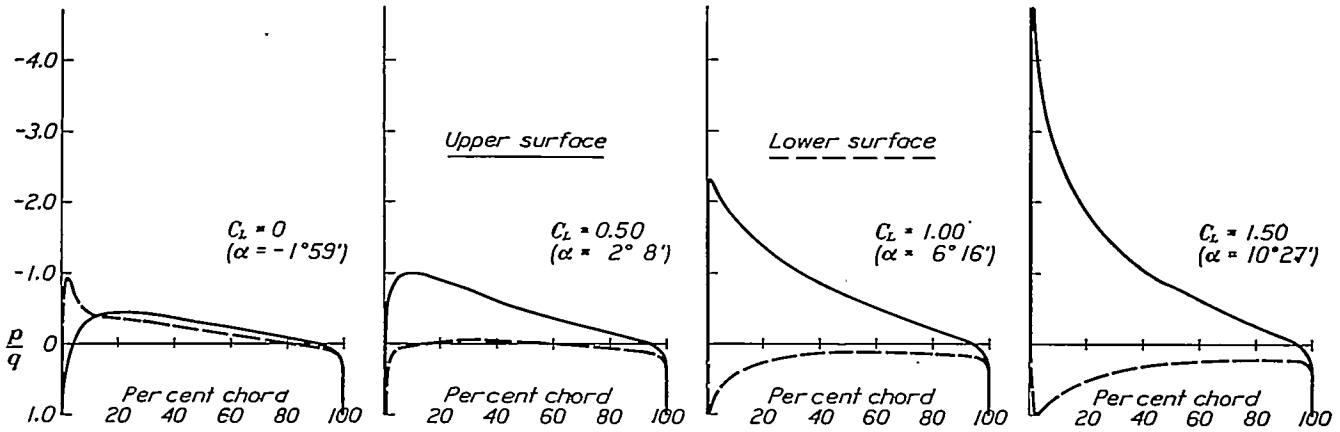

FIGURE 16.—Theoretical pressure distribution for the N.A.C.A. 2212 airfoil.

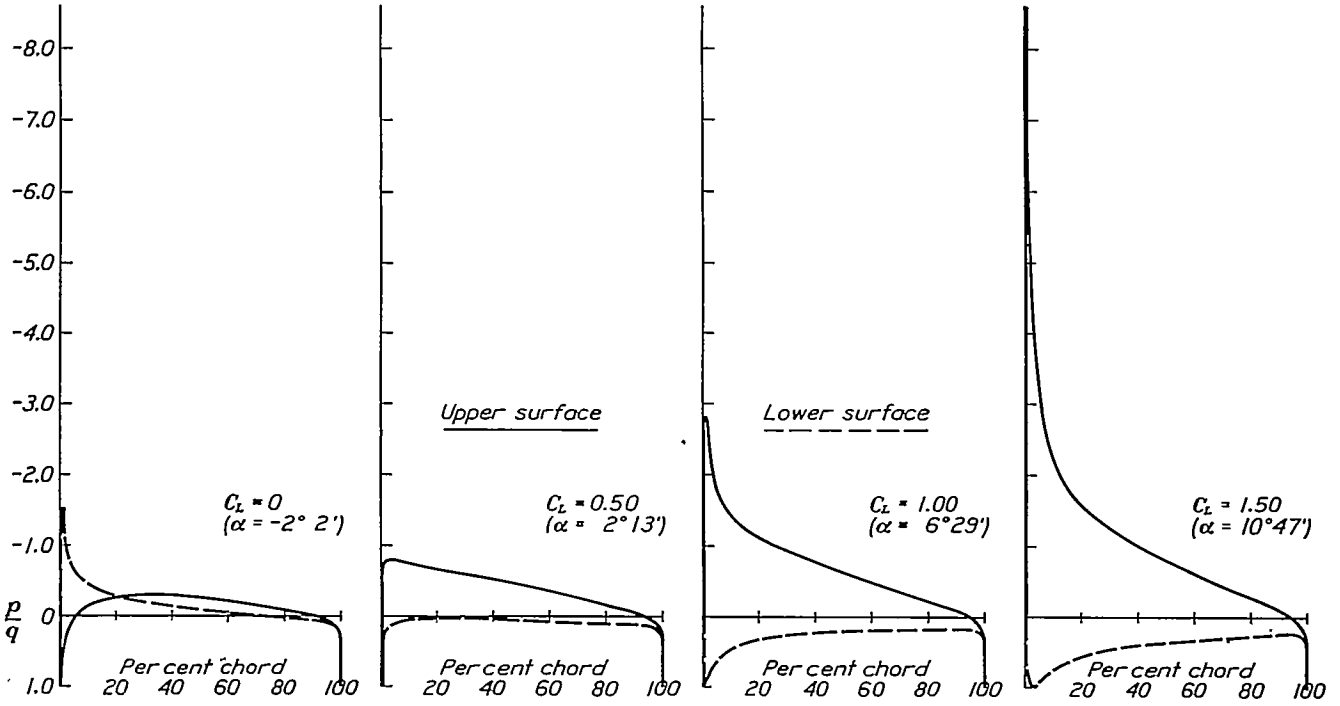

FIGURE 17.—Theoretical pressure distribution for the N.A.C.A. 2409 airfoil.

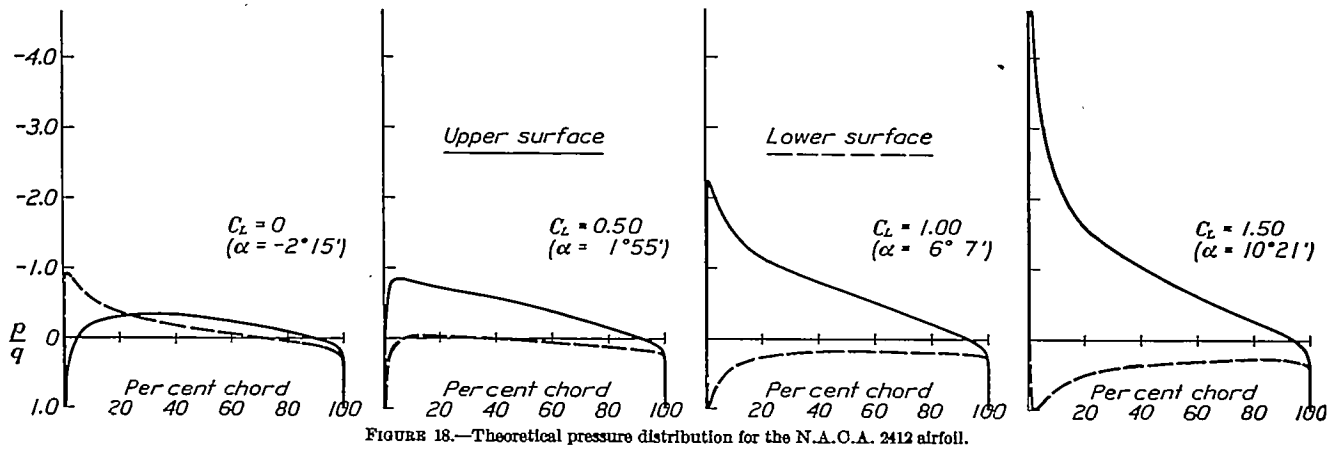

FIGURE 18.—Theoretical pressure distribution for the N.A.C.A. 2412 airfoil.

40768—34——29

airfoils used in practice without auxiliary devices, a pressure ratio p/q of about -3 or -4 is the maximum attained. It may be observed here that since the leading edge of the airfoil and the upper surface near the leading edge experience very large pressure gradients, they are critical regions, to be especially kept free from unnecessary protuberances and roughness.

It may be noted in the figures that very large pressure gradients exist in the region near the rear stagnation point, within the shadow of the 100 percent chord line. The rapid deceleration of fluid as thus shown to exist theoretically at the trailing edge most probably does not occur to any such extent in practice. The flow probably recombines at the trailing edge at velocities not much below normal, and the pressure curves are rounded off at a small positive pressure as shown in the figures. There is in this fact no essential violation of the Kutta condition for fixing the circulation, the primary purpose of which is only to avoid infinite velocities at the trailing edge.

Some effects of camber.—It may be observed that a property common to all airfoils is that the negative values of p/q mount rapidly near the leading edge on the upper surface after $C_L=1.00$ is exceeded. However, for the highly cambered airfoils, as the R.A.F. 19 and N.A.C.A. 6512, it may be noted that even for $C_L=1.50$ the p/q negative peak is but slightly above -2. These airfoils are high-lift airfoils, and the lift is well distributed over the whole chord. However, they have usually unfavorable pitching moments and rather wide travel of the center of pressure, as evidenced by the theoretical moment coefficients at zero lift, which are respectively -0.210 and -0.185.

Further effects of camber may be observed in figures 15, 18, 20, and 21 for the N.A.C.A. 0012, 2412, 4412, and 6512 airfoils, where in every case the maximum thickness is 12 percent of the chord and the maximum mean cambers are, respectively, 0, 2, 4, and 6 percent of the chord. The theoretical moment coefficients C_{M_F} are, respectively, 0, -0.055, -0.110, and -0.185.

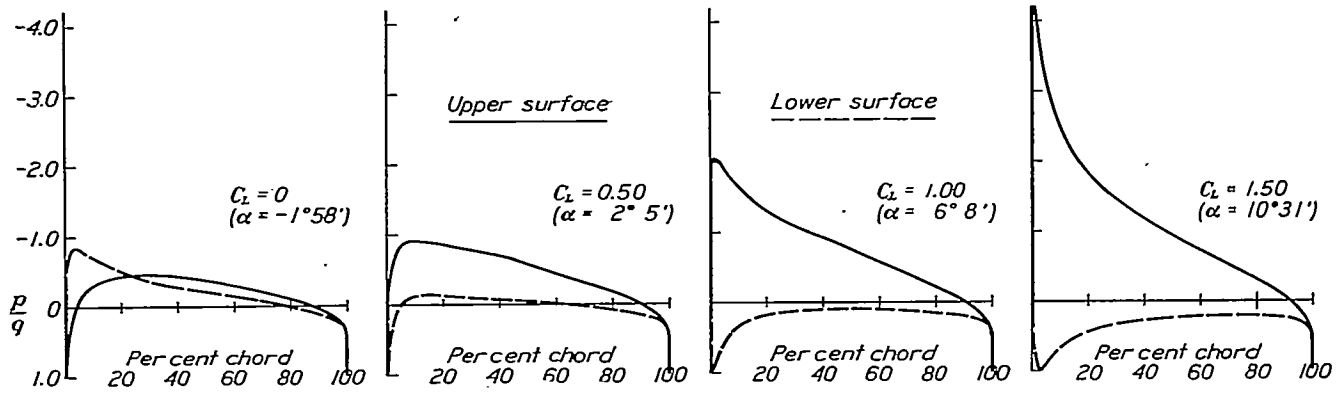

FIGURE 19.—Theoretical pressure distribution for the N.A.C.A. 2415 airfoil.

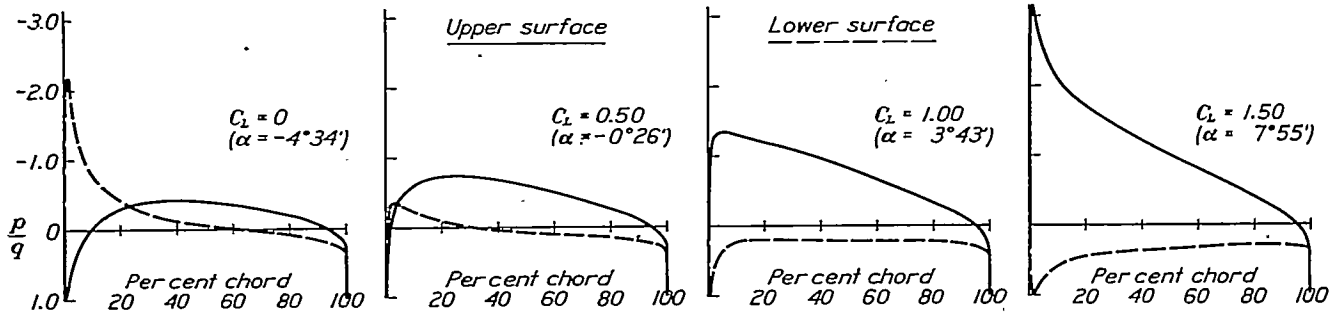

FIGURE 20.—Theoretical pressure distribution for the N.A.C.A. 4412 airfoil.

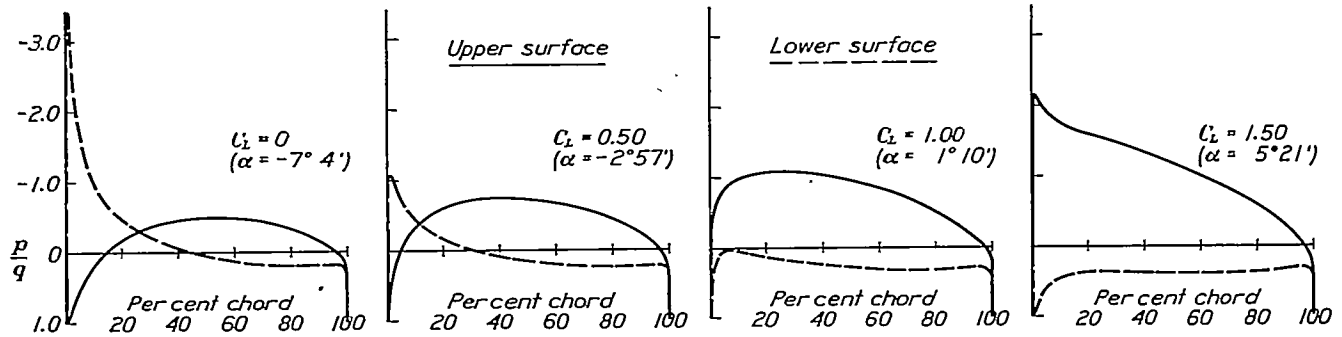

FIGURE 21.—Theoretical pressure distribution for the N.A.C.A. 6512 airfoil.

The ideal angle, also, increases with camber and, hence, the optimum lift coefficient increases in general with camber. We may observe that the high-cambered airfoils, and more especially thin high-cambered airfoils, are not efficient at low values of the lift coefficient, as is evidenced by the high negative peaks in the pressure distribution for zero lift. In fact, the flow around many high-cambered airfoils (for example, the R.A.F. 19) is known to burble on the under surface at low lift coefficients. Indeed, large gradients of deceleration of fluid may everywhere be associated with decreased efficiency. The bringing of pressure gradients and profile resistance into a precise correlation is a significant problem for further investigation. A uniform gradual change from velocity to pressure, as in figure 2 for the Clark Y airfoil at $C_L = 0.5$, gives probably the optimum lift distribution and occurs very nearly at the ideal angle of attack.

The experimental curves of lift coefficient against angle of attack for high-cambered airfoils like the R.A.F. 19 and N.A.C.A. 6512 are well rounded near maximum lift, whereas for airfoils like the N.A.C.A. 0010 and R.A.F. 15 they are likely to be sharp and jagged (reference 12). The former airfoils lose their lift rather gradually after maximum lift is attained, while for the latter airfoils this effect is likely to occur suddenly.

Effects of thickness.—In figures 17, 18, and 19 we may note some effects of the airfoil thickness. The N.A.C.A. 2409, 2412, and 2415 airfoils have a common mean-camber line and maximum thicknesses, respectively, of 9, 12, and 15 percent of the chord. For the N.A.C.A. 2415 it may be noted that the pressure on the under surface is generally less positive than for the 2412 and 2409. Also, we may observe that at lift coefficients $C_L = 1.00$ and $C_L = 1.50$ the down gradient of pressure along the first 15 percent of the chord is greatest for the 2409, while for the rest of the chord it is greatest for the 2415, indicating that an optimum effect for thickness lies perhaps between the extremes listed. The theoretical slope of the lift curve increases somewhat with thickness, and for the above airfoils has values of 6.75, 6.90, and 7.10, respectively. An experimental result that merits closer investigation is the fact that after a maximum thickness of about 12 percent is attained, $\frac{dC_L}{d\alpha}$ decreases somewhat with further increase in thickness (reference 12). A partial explanation lies in the fact that, in general, a thicker boundary layer exists on thick airfoils, decreasing their aerodynamic efficiency. It has, indeed, puzzled some observers employing various schemes for removing the boundary layer that the experimental slope of the lift curve for infinite aspect ratio often exceeds 2π, which is the value given by the approximate thin-airfoil theory. The average theoretical slope of the curves of lift against angle of attack for the airfoils listed in this report is approximately 6.90 or about $1.10 \times 2\pi$. This value is about 15 to 20 percent greater than the experimental value of the slope of the lift curve for infinite aspect ratio, and indicates that the airfoil is in general from about 80 to 85 percent efficient with regard to lift.

Moment properties.—The theoretical moment M_F is, in most of the cases studied in this paper, from about 10 to 20 percent greater than the experimental value of the moment for zero lift. (See references 12 and 13.) On the basis of (16), the position of the focus F, at which the theoretical moment is constant for all angles of attack, was calculated and is shown in the figures of the airfoils. (See fig. 1 and also table I.) In every case its abscissa is very nearly at 25 percent of the chord from the leading edge, the maximum for the airfoils considered being near 27 percent and the minimum near 24 percent of the chord line. However, it is important to note that, in general, the ordinate of F does not fall on the chord line but is usually located at a small distance from it.

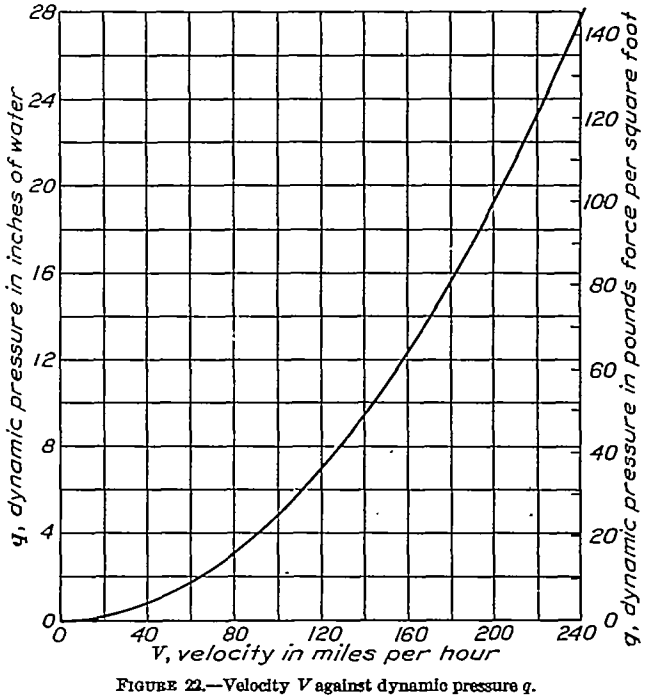

FIGURE 22.—Velocity V against dynamic pressure q.

The tendency for more constant center-of-pressure properties may be observed in figure 4 for the U.S.A. 27, where the lower-surface pressure curve has a small inflection or bend. For the N.A.C.A.-M6 (fig. 3), which theoretically has practically zero travel of the center of pressure, the double bend on the pressure curves at zero lift may be observed. Alternate regions of suction and pressure thus exist on each surface. The N.A.C.A.-CYH shows the same tendencies to a lesser degree. The double bend in the pressure-distribution curves is probably common to most reflexed airfoils.

Experimental results on the angles of zero lift show considerable discrepancies and indicate a change with the Reynolds Number. In general, the consistent experimental result is obtained that the angle of zero lift increases (algebraically) with increase in the Reynolds Number. For this reason we may only indicate a comparison with experimental values. The values listed in table I of this paper consistently fall within the range of values obtained by experiment and seem to agree more closely with experimental results obtained at moderate Reynolds Numbers (about 2×10^6) than with those taken at very large Reynolds Numbers. This fact should be investigated further.

CONCLUSIONS

The preceding discussion shows that, to a large extent, the general properties and characteristics of airfoils, such as effects due to camber, thickness, or change of shape, may be accounted for by the theoretical pressure-distribution curves. The theoretical pressure-distribution curves at definite lift coefficients may be safely used for structural-load considerations. A correlation between pressure gradients and profile resistance, affecting the efficiency of the airfoil, has been qualitatively indicated. Further theoretical and experimental investigations should be concerned with the significance of the differences between theory and experiment.

LANGLEY MEMORIAL AERONAUTICAL LABORATORY,
NATIONAL ADVISORY COMMITTEE FOR AERONAUTICS,
LANGLEY FIELD, VA., *June 2, 1933.*

REFERENCES

1. Blumenthal, Otto, and Trefftz, E.: Pressure Distribution on Joukowski Wings and Graphic Construction of Joukowski Wings. T.M. No. 336, N.A.C.A., 1925.
2. Perring, W. G. A.: The Theoretical Pressure Distribution around Joukowski Aerofoils. R. & M. No. 1106, British A.R.C., 1927.
3. Munk, Max M.: General Theory of Thin Wing Sections. T.R. No. 142, N.A.C.A., 1922.
4. Glauert, H.: A Theory of Thin Aerofoils. R. & M. No. 910, British A.R.C., 1924.
5. Theodorsen, Theodore: On the Theory of Wing Sections with Particular Reference to the Lift Distribution. T.R. No. 383, N.A.C.A., 1931.
6. Theodorsen, Theodore: Theory of Wing Sections of Arbitrary Shape. T.R. No. 411, N.A.C.A., 1931.
7. Theodorsen, T., and Garrick, I. E.: General Potential Theory of Arbitrary Wing Sections. T.R. No. 452, N.A.C.A., 1933.
8. Jacobs, Eastman N., Stack, John, and Pinkerton, Robert M.: Airfoil Pressure Distribution Investigation in the Variable Density Wind Tunnel. T.R. No. 353, N.A.C.A, 1930.
9. Briggs, L. J., and Dryden, H. L.: Pressure Distribution over Airfoils at High Speeds. T.R. No. 255, N.A.C.A., 1927.
10. Glauert, H.: The Effect of Compressibility on the Lift of an Aerofoil. R. & M. No. 1135, British A.R.C., 1928.
11. Anderson, Raymond F.: The Aerodynamic Characteristics of Airfoils at Negative Angles of Attack. T.N. No. 412, N.A.C.A., 1932.
12. Jacobs, Eastman N., Ward, Kenneth E., and Pinkerton, Robert M.: The Characteristics of 78 Related Airfoil Sections from Tests in the Variable Density Wind Tunnel. T.R. No. 460, N.A.C.A., 1933.
13. Jacobs, Eastman N., and Anderson, Raymond F.: Large-Scale Aerodynamic Characteristics of Airfoils as Tested in the Variable Density Wind Tunnel. T.R. No. 352, N.A.C.A., 1930.

TABLE I

THEORETICAL CONSTANTS FOR THE TWENTY AIRFOILS

Airfoil	$e^{i\beta_0}$	c	$\frac{d C_L}{d \sin(\alpha+\beta)}$	β	γ	b^2	$\frac{b^2}{e^{i\beta_0}}$	C_{MI}	α_I	C_{mI}	m	δ	λ
				° ′	° ′				° ′			° ′	° ′
Clark Y	1.112	4.031	6.93	3 35	0 24	0.995	0.894	−0.085	0 38	0.51	0.110	46 50	1 59
N.A.C.A.—M6	1.117	4.040	6.95	0 36	0 42	.966	.864	.003	1 0	.19	.079	29 0	0 0
U.S.A. 27	1.115	4.024	6.96	4 31	0 57	.990	.888	−.095	1 16	.69	.117	58 0	0 38
U.S.A. 35B	1.109	4.038	6.90	4 14	0 29	1.000	.900	−.100	0 49	.60	.127	47 10	1 36
N. 22	1.118	4.036	6.96	4 7	0 18	1.000	.894	−.102	0 35	.56	.125	48 0	1 50
Göttingen 387	1.153	4.064	7.12	5 23	0 39	1.000	.867	−.125	0 55	.77	.173	46 10	2 0
Göttingen 398	1.142	4.040	7.09	4 25	0 37	1.002	.878	−.102	0 35	.61	.140	48 30	2 3
N.A.C.A.—CYH	1.114	4.029	6.95	1 52	0 44	1.000	.897	−.017	1 0	.34	.094	40 0	0 52
C 72	1.107	4.029	6.91	4 13	0 11	.990	.900	−.107	0 25	.55	.113	47 30	2 0
Boeing 103 A	1.093	4.022	6.84	2 48	0 13	.985	.900	−.075	1 17	.48	.092	49 20	1 11
R.A.F. 15	1.071	4.012	6.71	2 35	0 37	1.017	.950	−.052	1 18	.47	.068	63 10	0 0
R.A.F. 19	1.116	4.022	6.97	8 56	1 26	1.053	.944	−.210	2 0	1.30	.200	68 30	0 24
N.A.C.A. 0010	1.092	4.023	6.82	0 0	0 0	.990	.910	.000	0 0	.00	.051	0 0	0 0
N.A.C.A. 0012	1.112	4.033	6.93	0 0	0 0	.995	.900	.000	0 0	.00	.080	0 0	0 0
N.A.C.A. 2212	1.119	4.034	6.97	1 59	0 30	.997	.892	−.039	1 12	.38	.057	60 10	0 0
N.A.C.A. 2409	1.083	4.019	6.78	2 2	0 6	1.000	.922	−.052	0 22	.28	.065	45 50	0 0
N.A.C.A. 2412	1.103	4.034	6.87	2 15	0 13	.998	.905	−.055	0 20	.30	.085	28 30	0 0
N.A.C.A. 2415	1.142	4.052	7.10	1 53	0 6	.997	.875	−.050	0 32	.30	.116	25 20	0 0
N.A.C.A. 4412	1.114	4.034	6.94	4 34	0 21	.995	.895	−.110	0 38	.62	.128	49 50	0 0
N.A.C.A. 6512	1.119	4.034	6.98	7 4	0 0	.993	.887	−.185	0 19	.89	.148	65 30	0 0

NOTE.—The values of the angles listed in table I with respect to the x axis may be converted to values with respect to the standard chord by the addition of λ.

TABLE II

CLARK Y AIRFOIL

UPPER SURFACE

Percent c	y in percent c	x	y	$\sin^2\theta$	$\sinh^2\psi$	θ	ψ	ϵ	ψ'	ϵ'	k	$\phi=\theta+\epsilon$	
												radians	° ′
0	0	2.030	0	0	0.0302	0	0.173	−0.0846	0.035	0.070	6.842	−0.085	−4 51
1.25	1.99	1.983	.0802	.0486	.0331	.222	.182	−.0735	.067	.080	4.192	.1485	8 31
2.50	3.09	1.933	.1246	.1007	.0386	.323	.195	−.0640	.110	.114	3.299	.259	14 50
5.0	4.57	1.834	.184	.194	.0436	.456	.207	−.0501	.067	.133	2.578	.406	23 17
7.5	5.61	1.736	.226	.280	.0457	.557	.212	−.0362	.044	.150	2.240	.521	29 51
10	6.45	1.636	.260	.361	.0468	.644	.215	−.0225	.021	.145	1.993	.622	35 38
15	7.70	1.436	.310	.503	.0474	.793	.216	−.0005	.008	.133	1.691	.793	45 25
20	8.55	1.236	.345	.635	.0467	.922	.214	.0163	−.017	.133	1.525	.939	53 47
30	9.23	.834	.372	.833	.0415	1.150	.202	.0430	−.067	.111	1.318	1.193	68 20
40	9.28	.430	.374	.955	.0366	1.368	.190	.0635	−.067	.086	1.210	1.422	81 29
50	8.74	.0263	.352	.998	.0311	1.530	.175	.0772	−.080	.073	1.172	1.607	92 6
60	7.72	−.378	.311	.965	.0251	1.759	.158	.0918	−.089	.050	1.169	1.850	106 2
70	6.26	−.783	.252	.850	.0187	1.969	.136	.101	−.100	.040	1.235	2.070	118 37
80	4.47	−1.189	.180	.651	.0125	2.203	.112	.106	−.114	.013	1.374	2.309	132 18
90	2.40	−1.595	.0968	.348	.0063	2.489	.0793	.105	−.114	−.022	1.766	2.594	148 39
95	1.26	−1.798	.0508	.1945	.0032	2.685	.0566	.0961	−.100	−.057	2.346	2.781	159 20
100	0	−2.001	0	0	.0010	3.142	.0310	.0626	−.044	−.077	large	3.204	183 36

LOWER SURFACE

0	0	2.030	0	0	0.0302	6.283	0.173	−0.0846	0.035	0.070	6.842	6.199	−4 51
1.25	−1.53	1.983	−.0617	.0429	.0221	6.074	.148	−.103	.171	.055	4.535	5.966	−18 8
2.50	−1.94	1.933	−.0782	.0385	.0173	5.981	.131	−.110	.149	−.011	3.344	5.871	−23 35
5.0	−2.40	1.834	−.0968	.178	.0131	5.847	.114	−.103	.123	−.024	2.463	5.739	−31 10
7.5	−2.61	1.736	−.105	.265	.0104	5.743	.102	−.108	.100	−.031	2.044	5.637	−37 1
10	−2.73	1.636	−.110	.347	.0087	5.653	.0932	−.103	.092	−.033	1.795	5.550	−41 59
15	−2.83	1.436	−.114	.498	.0035	5.499	.0805	−.0975	.080	−.044	1.491	5.402	−50 29
20	−2.78	1.236	−.112	.630	.0049	5.368	.0699	−.0918	.073	−.044	1.331	5.275	−57 48
30	−2.47	.834	−.0998	.833	.0030	5.133	.0548	−.0800	.057	−.057	1.145	5.053	−70 27
40	−2.12	.430	−.0855	.957	.0019	4.920	.0436	−.0670	.044	−.060	1.036	4.853	−81 55
50	−1.78	.0263	−.0718	1.000	.0013	4.712	.0361	−.0538	.040	−.057	1.036	4.659	−93 4
60	−1.43	−.378	−.0576	.962	.0003	4.516	.0283	−.0425	.031	−.057	1.057	4.473	−103 41
70	−1.09	−.783	−.0439	.842	.0005	4.304	.0224	−.0282	.025	−.037	1.130	4.276	−114 53
80	−.75	−1.189	−.0302	.643	.0003	4.030	.0173	−.0080	.014	−.030	1.276	4.022	−123 31
90	−.40	−1.595	−.0161	.361	.0002	3.786	.0141	.0033	.017	−.035	1.674	3.794	−142 38
95	−.23	−1.798	−.0093	.190	.0001	3.593	.0100	.0255	.000	−.100	2.295	3.618	−152 40
100	0	−2.001	0	0	.0010	3.142	.0310	.0626	−.044	−.077	large	3.204	−176 24